

Kapp, P., et al., 2023, Laramide bulldozing of lithosphere beneath the Arizona transition zone, southwestern United States: *Geology*, <https://doi.org/10.1130/G51194.1>

## Supplemental Material

**Analytical methods, thermal modeling information, Figures S1–S9, and Tables S1–S6.**

## **Zircon U-Pb LA-ICP-MS Methodology**

Sample A (manuscript name; 9.8.20.2PK is primary sample name) was analyzed following standard procedures for zircon U-Pb geochronology by LA-ICP-MS at the Arizona Laserchron Center (ALC; [www.laserchron.org](http://www.laserchron.org); Gehrels et al., 2008, Gehrels and Pecha, 2014).

### *Zircon Separation, Mount Preparation, and Data Acquisition*

Zircons were separated from ~1 kg of rock using traditional methods of crushing, water separation, magnetic separation, and heavy liquids separation (Gehrels et al., 2008). Grains were picked and mounted in epoxy with primary reference material FC-1 (isotope dilution-thermal ionization mass spectrometry [ID-TIMS] age of  $1099.0 \pm 0.6$  Ma), secondary reference material SL-F (ID-TIMS age of  $555.86 \pm 0.68$  Ma), and tertiary reference material R33 (ID-TIMS age of  $419.3 \pm 0.4$  Ma) (Paces and Miller, 1993; Black et al., 2004; S. Bowring, 2017, personal communication with George Gehrels regarding unpublished report titled “MIT LA SRI LAN F” that details the ID-TIMS age for a natural reference material). The epoxied mount was polished to maximize the exposed surface area of zircon and back-scattered electron images were produced using a Hitachi 3400N scanning electron microscope as reference images for laser spot placement prior to data acquisition.

Igneous zircon U-Pb analysis by LA-ICP-MS was conducted at the ALC following the methods of Gehrels et al. (2008), Gehrels and Pecha (2014), and Pullen et al. (2018).

Instrumentation consisted of Photon Machines Analyte-G2 ArF 193 nm excimer laser with a HelEx2 ablation cell connected to a Thermo Element2 high-resolution single-collector ICP-MS via an aerosol rapid introduction system. In total, 35 unknowns, 18 primary reference materials (FC-1), 9 secondary reference materials (SL-F), and 5 tertiary reference materials (R33) were analyzed using sample-standard bracketing to monitor instrument drift over the data acquisition

session by checking for systematic shifts in ages of the reference materials relative to their accepted ID-TIMS values. Prior to the first analysis, all laser spots were ablated with a 50  $\mu\text{m}$  cleaning shot to remove common Pb and/or surface contaminants. Each spot was then analyzed using a 30  $\mu\text{m}$  laser spot and ablated to a depth of  $\sim 15$   $\mu\text{m}$ . Ablated material was carried by helium gas into the plasma source of the mass spectrometer and isotopes of U, Th, Pb, and Hg were detected via dual mode secondary electron multiplier and analyzed in sequence via peak-hopping.

### *Data Reduction*

Isotopic data were reduced at the ALC using the in-house *Excel*-based program *E2agecalc*. Before raw data are converted to isotopic ratios of interest ( $^{206}\text{Pb}/^{238}\text{U}$ ,  $^{206}\text{Pb}/^{207}\text{Pb}$ , and  $^{208}\text{Pb}/^{232}\text{Th}$ ), ion intensities of individual isotopes are first corrected by subtracting backgrounds, accounting for isobaric interferences, and correcting for common Pb (Stacey and Kramers, 1975). The preliminary isotopic ratios from analyses of primary reference materials are then compared to accepted values to determine fractionation factors for  $^{206}\text{Pb}/^{238}\text{U}$ ,  $^{206}\text{Pb}/^{207}\text{Pb}$ , and  $^{208}\text{Pb}/^{232}\text{Th}$ , and the fractionation factor is applied to all analyses using a sliding-window average. Uncertainties are then propagated following the methods of Gehrels et al. (2008) and Gehrels and Pecha (2014).

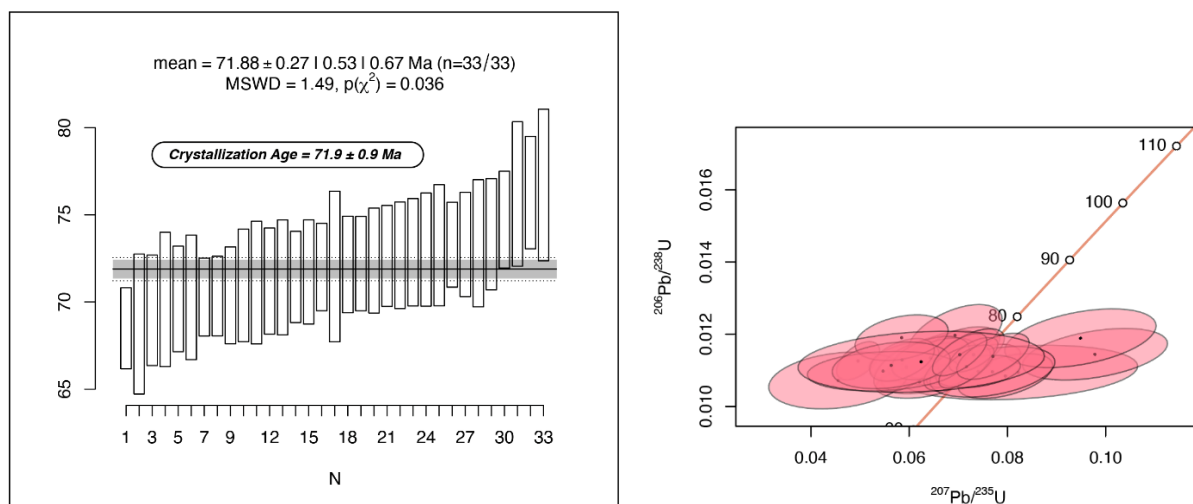


**Figure S1.** Weighted mean age and Concordia plots for Sample A. The large uncertainties in the  $^{207}\text{Pb}/^{238}\text{U}$  measurements are because of low U concentrations (generally <75 ppm) and the relatively young age of the sample, which leads to large uncertainties in measuring  $^{207}\text{Pb}$  and the common Pb correction.

#### **$^{40}\text{Ar}/^{39}\text{Ar}$ thermochronology methods**

Four  $^{40}\text{Ar}/^{39}\text{Ar}$  incremental heating experiments were conducted on biotite from two Proterozoic granite samples in the Arizona Transition Zone (Bradshaw Mountains) at the Arizona Noble Gas Laboratory at the University of Arizona. Mineral separates were isolated from the rocks by crushing, sieving from 350 to 500  $\mu\text{m}$ , and then hand-picked under a binocular microscope to isolate single grains. The purified separates were wrapped in aluminum foil, placed in 2.5 cm aluminum disks, and irradiated along with the 28.201 Ma Fish Canyon sanidine standard (Kuiper et al., 2008) at the Oregon State University TRIGA reactor in the Cadmium-Lined In-Core Irradiation Tube (CLICIT). Aliquots (0.5-1 mg) and single crystals of biotite were placed in a 5 mm well within a copper planchette and incrementally heated with a Teledyne Instruments 55 W  $\text{CO}_2$  laser. Extracted gas was cleaned for 20-30 mins using two SAES GP50

getter at 450°C, one SAES NP10 getter at room temperature, and an Edwards Polycold® PCC Compact Cooler maintained at -90 °C before being analyzed using a Thermo Fisher Scientific Argus VI multicollector noble gas mass spectrometer.  $^{40}\text{Ar}/^{39}\text{Ar}$  dates are calculated using the decay constants of Min et al. (2000) and analytical uncertainties, including J contributions, are reported at  $2\sigma$ . Samples were corrected using an atmospheric  $^{40}\text{Ar}/^{36}\text{Ar}$  ratio of  $298.56 \pm 0.31$  (Lee et al., 2006). Data reduction was performed using Pychron software (Ross, 2019).

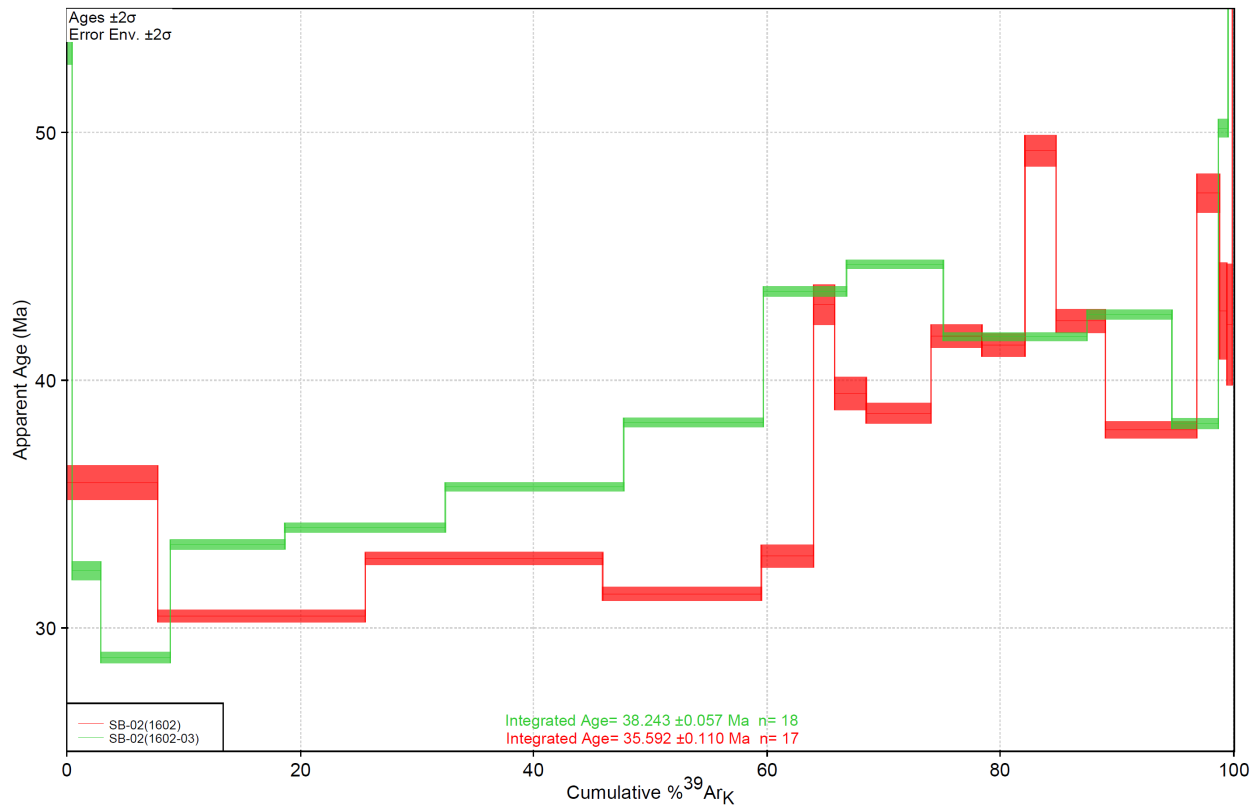


**Figure S2.** Biotite  $^{40}\text{Ar}/^{39}\text{Ar}$  apparent age spectra for one single-crystal and one 0.5 mg aliquot from manuscript Sample E (original sample name SB-02).

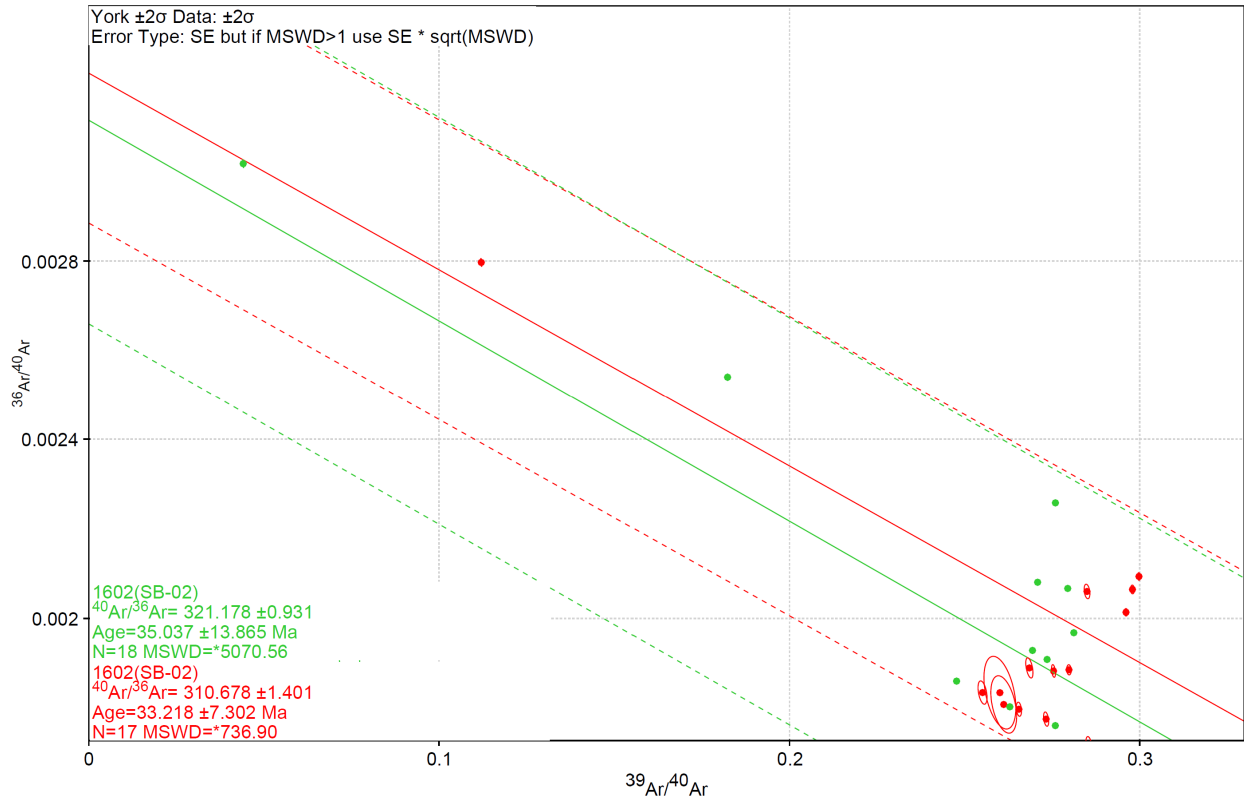


**Figure S3.** Inverse isochron plots for manuscript Sample E (original Sample SB-02). Low  $^{36}\text{Ar}$  abundances preclude calculation of well-defined isochrons with little spread in  $^{36}\text{Ar}/^{40}\text{Ar}$ .

$^{40}\text{Ar}/^{36}\text{Ar}$  intercepts (311, 320) are in excess of modern atmosphere ( $^{40}\text{Ar}/^{36}\text{Ar} = 298.56$ , Lee et al., 2006) although given the poorly defined isochrons the presence of excess Ar in this sample is questionable.

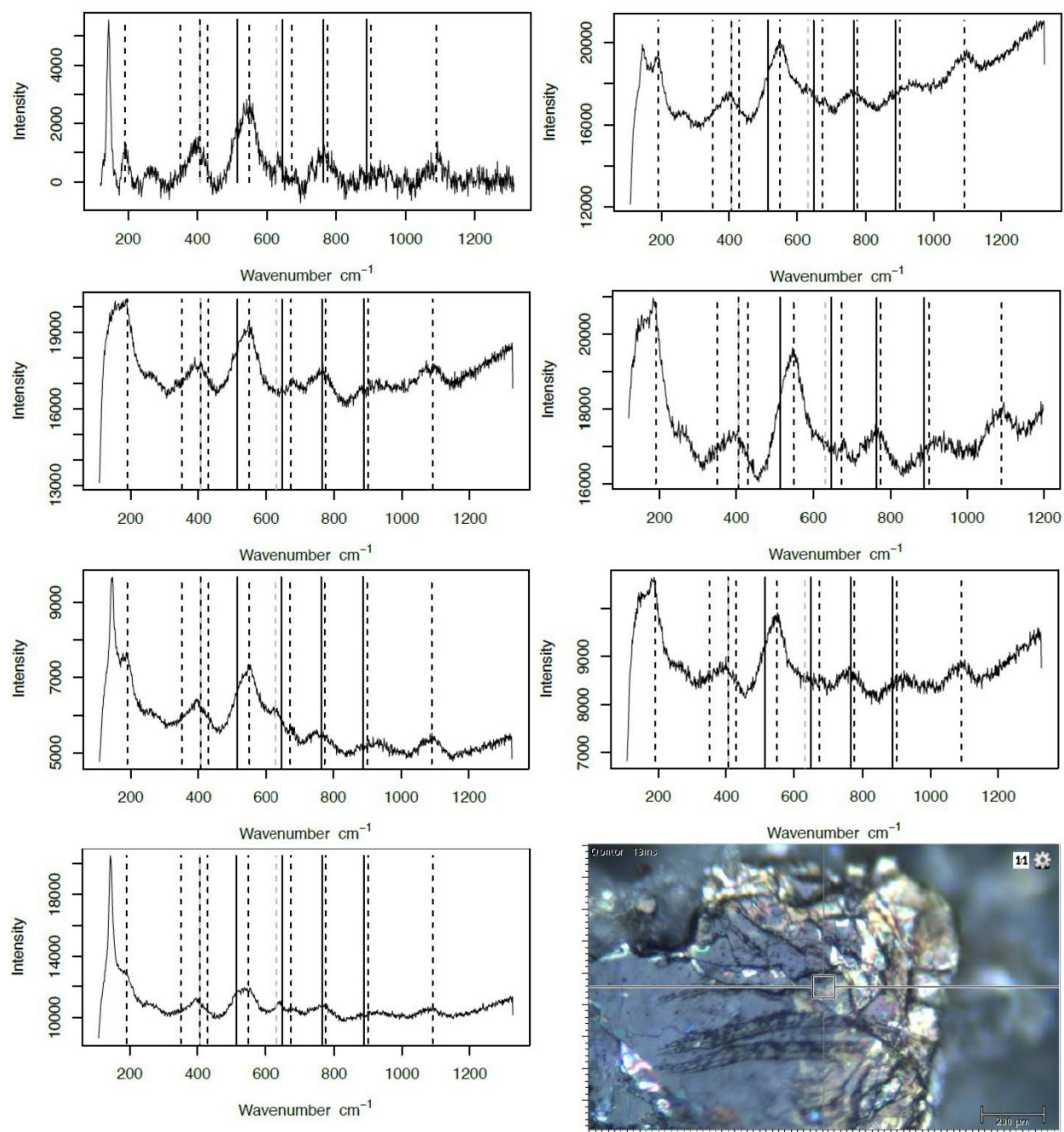


**Figure S4.** Raman spectroscopy results for biotite from Sample E (original Sample SB-02). The spectra show signs of alteration from pure biotite (peaks corresponding to solid lines; Dumańska-Slowik et al., 2015) to vermiculite (peaks corresponding to dashed lines; Wang et al., 2015; Ritz and Valášková, 2018). Lower right is a representative reflected light image.

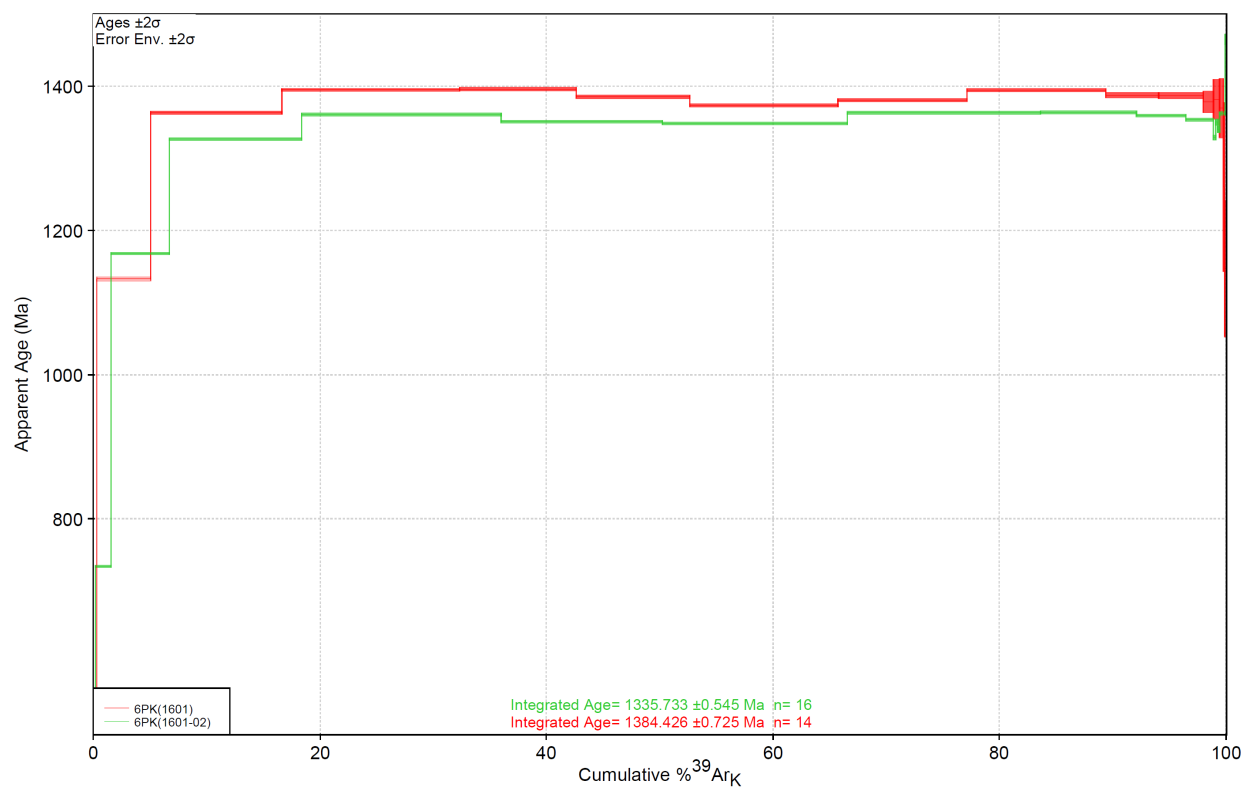


**Figure S5.** Biotite  $^{40}\text{Ar}/^{39}\text{Ar}$  apparent age spectra for one single-crystal and one 1 mg aliquot from manuscript Sample F (original sample name 10.10.20.6PK).



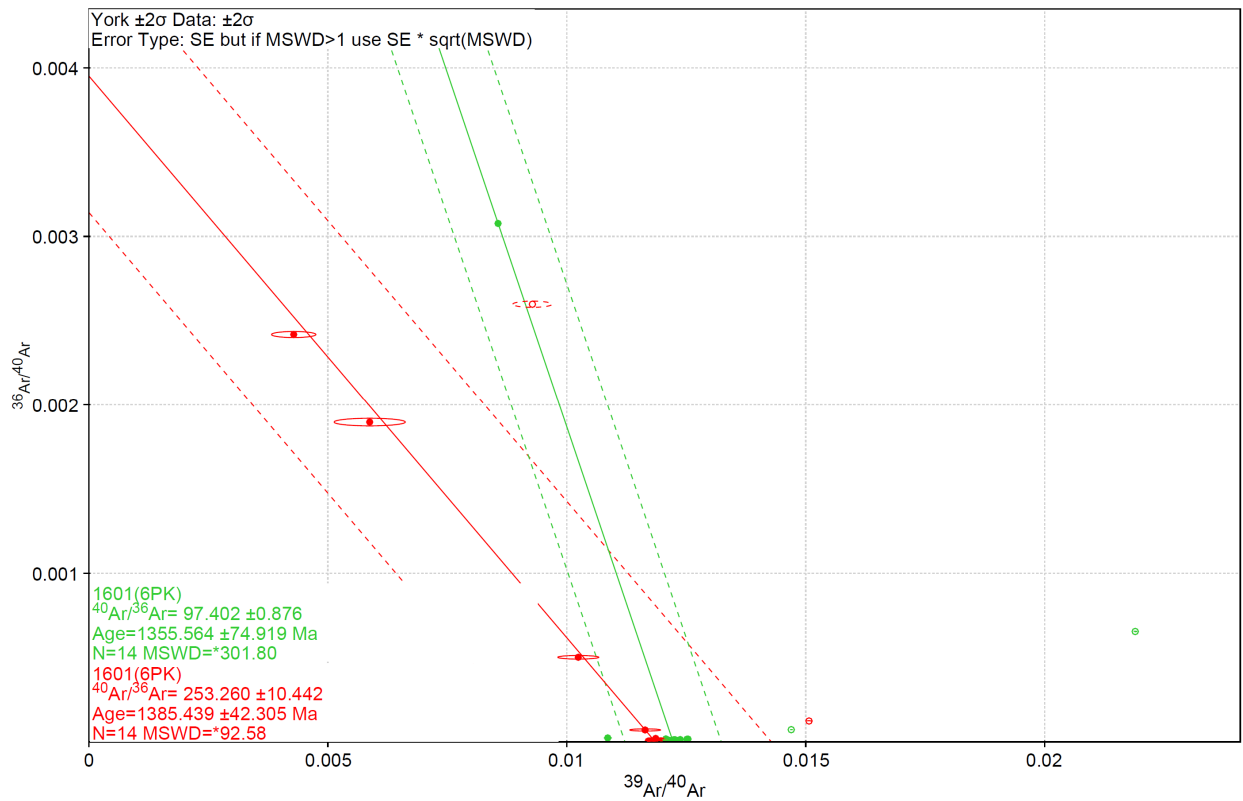


**Figure S6.** Inverse isochron plots for manuscript Sample F (original sample name 10.10.20.6PK).

### Apatite fission-track methods

The fission-track thermochronometer relies on the spontaneous fission decay of  $^{238}\text{U}$  (Hurford and Green, 1983). Spontaneous fission within apatite is annealed between temperatures of  $\sim 120$ – $60$  °C, making this system useful for constraining upper-crustal cooling (e.g., Braun et al., 2006, and references within). The fission-track analyses were performed at the University of Arizona Fission Track Laboratory. Apatites were extracted via standard heavy mineral techniques. Apatite crystals are mounted in epoxy and polished to reveal their internal sections, with spontaneous fission-tracks revealed through etching with 5.5 M nitric acid for 20 s at 21 °C before irradiation (after Donelick et al., 2005). Samples were analyzed via the external detector method (Gleadow et al., 1976) which utilizes low uranium muscovite mica detectors, and were

irradiated at the Oregon State University Triga Reactor, Corvallis, USA. The total neutron fluence was checked using CN5 U-doped. Following irradiation, the mica sheets were etched in 40% hydrofluoric acid for 45 min at 21 °C (after Donelick et al., 2005). Apatite fission-tracks were counted using an Olympus BX51 microscope with an associated digitizing tablet and computer controlled stage (Kinetek) in Tucson at x1600 magnification. Confined fission-track length distributions were obtained to determine cooling rates; mean track lengths (MTLs) of  $>13.5 \mu\text{m}$  are considered to be reflective of rapid cooling (Ketcham et al., 2007). The central ages were calculated by using the  $\zeta$ -method after Hurford and Green (1983) (Table 2). Radial plots were produced using radial plotter (Vermeesch, 2009). Apatite fission-track ages were calculated using a  $\zeta$ -value of  $341.6 \pm 8.5$  (GJ).

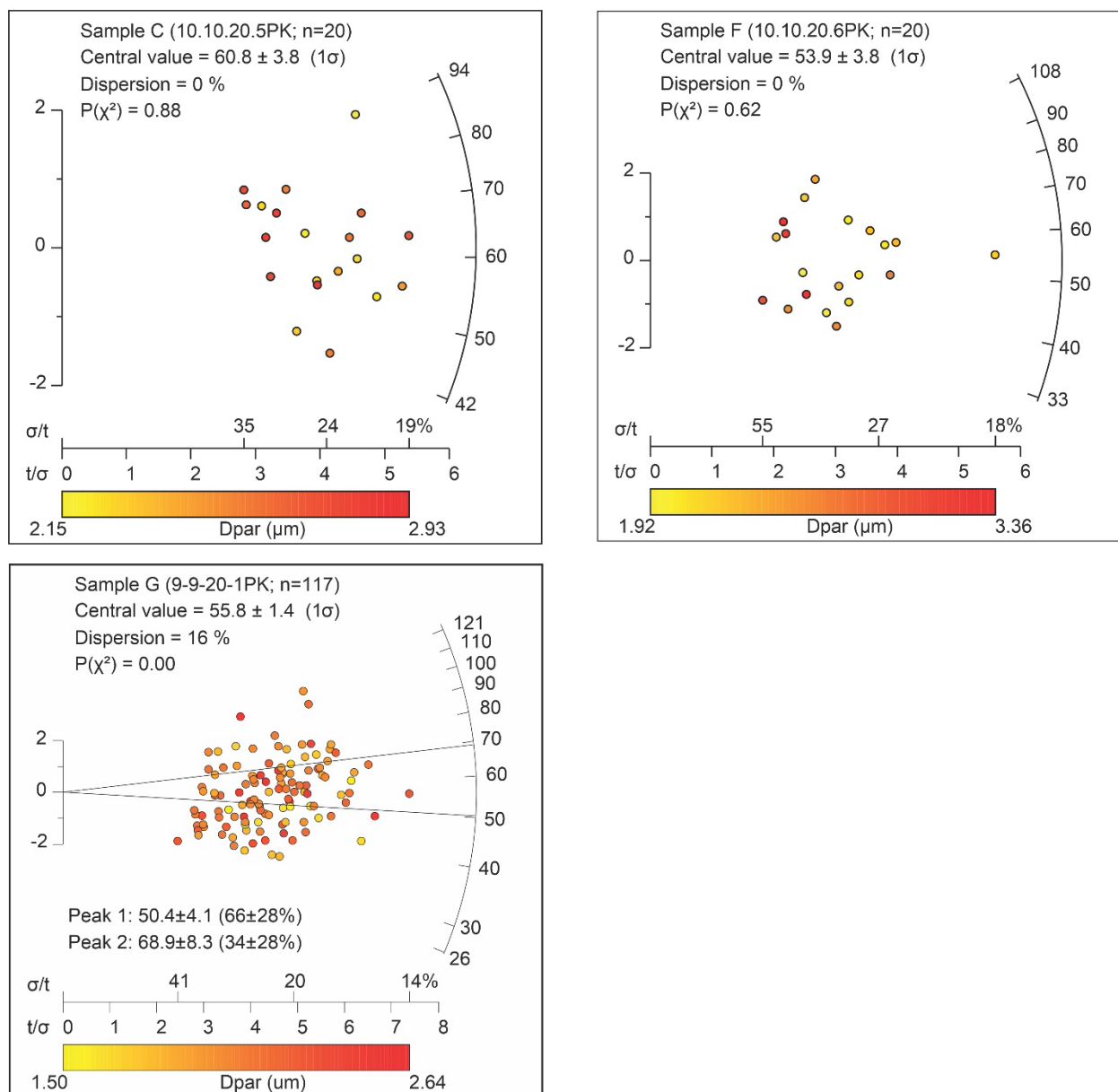


**Figure S7.** Radial fission-track plots for Samples C, F, and G.

### Zircon and apatite (U-Th-[Sm])/He methods

All (U-Th)/He analyses were performed at the University of Arizona Noble Gas Laboratory. Apatite and zircon crystals were extracted from crushed samples following routine mineral separation protocols, and individually reviewed for inclusions, imperfections, fractures, coatings, and fragmentation. Crystals were photographed and measured under a high-powered

stereo-zoom microscope on two sides. They were then packed individually in Nb envelopes and degassed by laser heating up to ~900-1300 °C, with higher temperature used for zircon degassing. Reference Durango standards were analyzed at the beginning, middle, and end of each analysis run along with unknowns to account for variation in isotopic fractionation or sensitivity bias.  $^4\text{He}$  was measured by isotope dilution with a quadrupole mass spectrometer. Nb envelopes and included apatite/zircon crystals were then transferred to Teflon vials and dissolved. U-Th-Sm (plus Ca in apatite and Zr in zircon) were measured by isotope dilution on a high-resolution single-collector sector ICP-MS. We applied corrections to account for alpha-ejection using measurements of crystal dimension (assuming hexagonal prism geometry, for apatite, and orthorhombic prism with pyramidal terminations, for zircons) (Farley, 2002), with updated alpha-ejection correction calculations for fragmented grains (He and Reiners, 2022). Detailed procedures can be found in Reiners et al. (2018), or lab protocols posted on the University of Arizona helium laboratory website (<https://www.geo.arizona.edu/~reiners/arhdl/methodsalready.pdf>), with the exception of the updated fragmentation correction referenced above (He and Reiners, 2022).

We report all single-aliquot analyses in supplementary Table S4 and note in red any anomalous data that were not included in the calculation of summary statistics for any given sample. Because samples yielded few zircon grains, no zircon analyses were excluded from consideration. We also report the mean, median, and for apatite helium analyses, the first quartile date (FQD) for each sample (He et al., 2021), the latter to account for the far higher likelihood of errors that skew corrected dates to be many multiples older (in particular, the effect of helium implantation from adjacent high-eU accessory minerals like zircon into low-eU apatite crystals, i.e. “parentless” helium) than errors that skew dates to be younger in apatite helium samples

(Spiegel et al., 2009; Gautheron et al., 2012; He et al., 2021; Flowers et al., 2023). Uncertainties ( $1\sigma$ ) were calculated using non-parametric bootstrapping (with resampling,  $n = 10,000$ ), which has the advantage of avoiding the assumption that the underlying distribution is distributed normally (He et al., 2021).

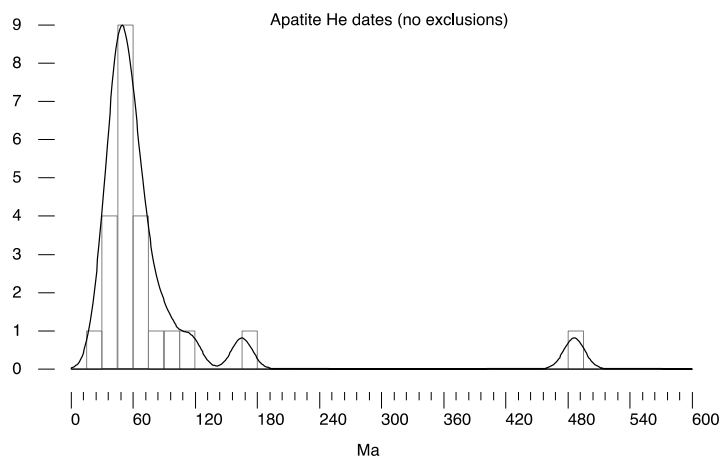
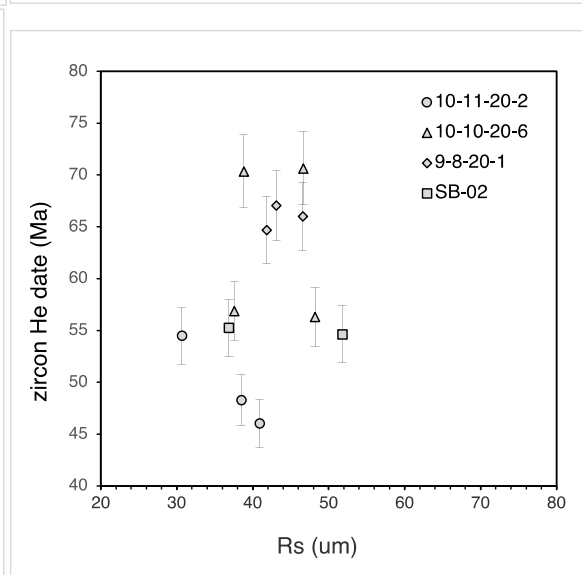
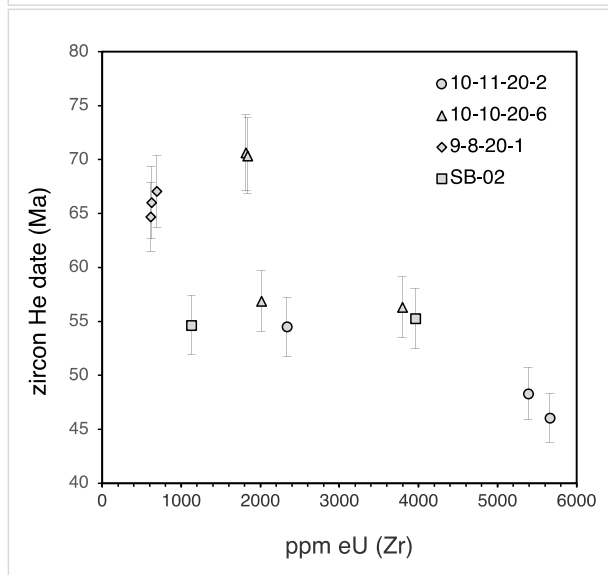
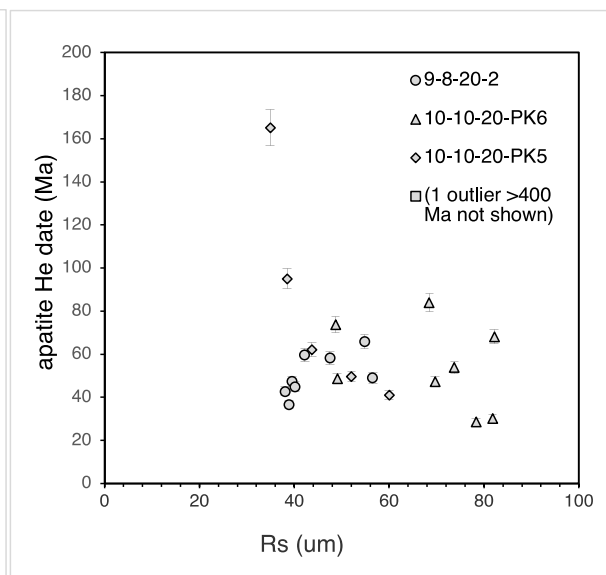
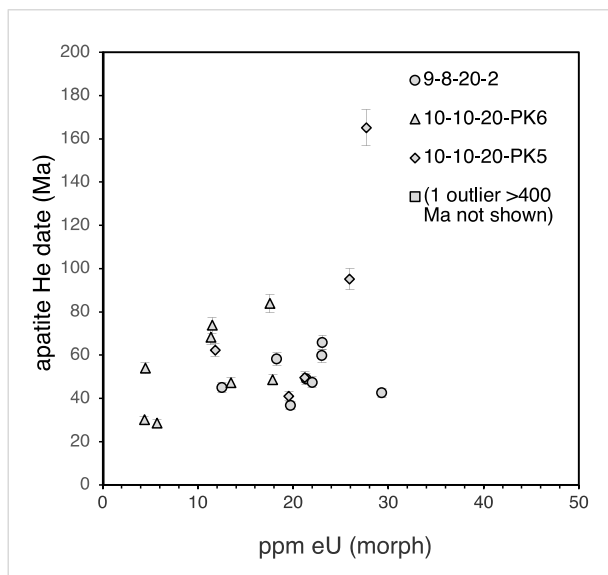


**Figure S8.** Supplementary apatite and zircon helium figures. eU – effective uranium concentration; Rs – sphere-equivalent radius.

### **Thermal history modeling:**

Inverse thermal history modeling using QTQt 5.7.0 (Gallagher, 2012) was conducted on manuscript Sample C and Sample F in the Bradshaw Mountains and previously published apatite (U-Th-Sm)/He data from three samples analyzed along the southern margin of the Colorado Plateau (CP-0501, CP-06-19, CP-06-20; Flowers et al., 2008). The QTQt software applies a Bayesian trans-dimensional approach to Markov Chain Monte Carlo statistics (Gallagher 2012) to produce a cooling evolution of the sample that predicts the measured data by applying the AFT annealing model after Ketcham et al. (2007) and the AHe diffusion model after Flowers et al. (2009). Our approach used an initial unconstrained run to explore the statistical space, that was then followed by adjustments to the search parameters as well as the addition of geological constraints. A large number of iterations ( $n \gg 100,000$ ) were run to generate a range of models that can constrain a probability distribution. From the obtained probability distribution an individual thermal history can be selected, such as the maximum likelihood as well as an “expected” (weighted mean) paths. We followed acceptance rates for models that were between 0.1 and 0.6 and with a birth-death ratio of  $\sim 1$ . Model input data, assumptions, uncertainties, and other system- and model-specific parameters are provided in Table S6 following the framework established by Flowers et al. (2015).

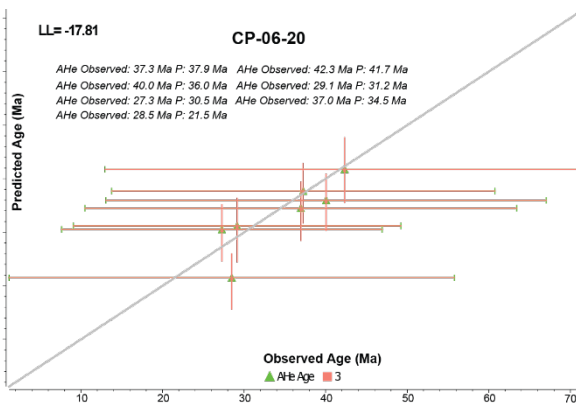
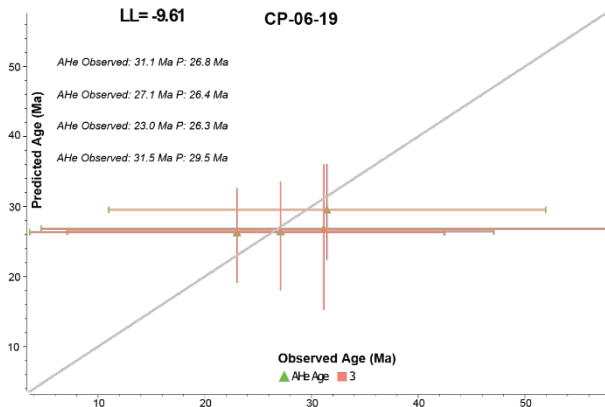
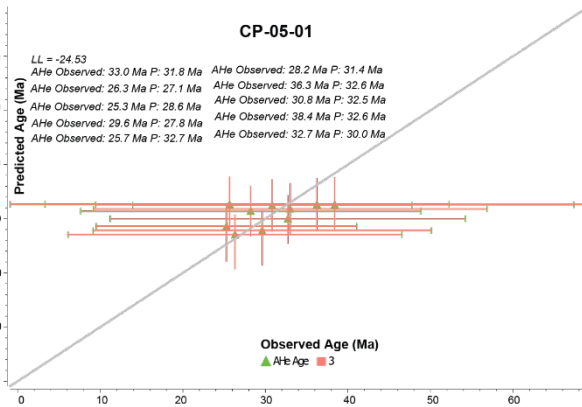
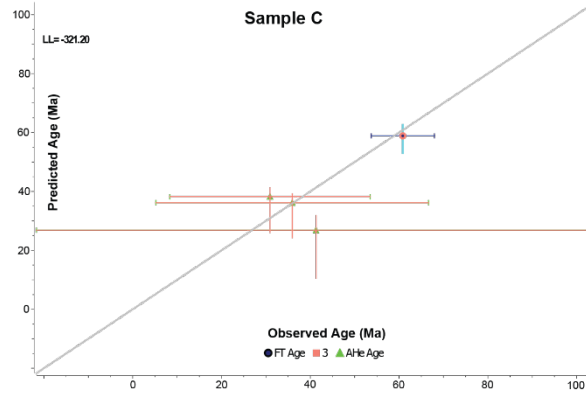
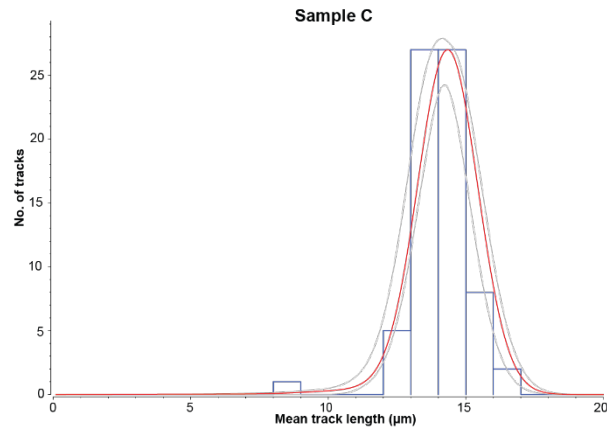
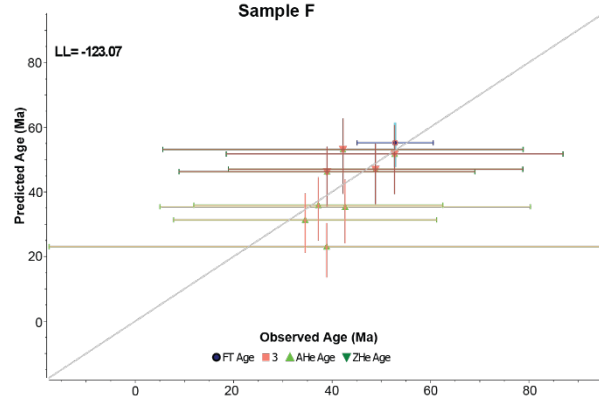
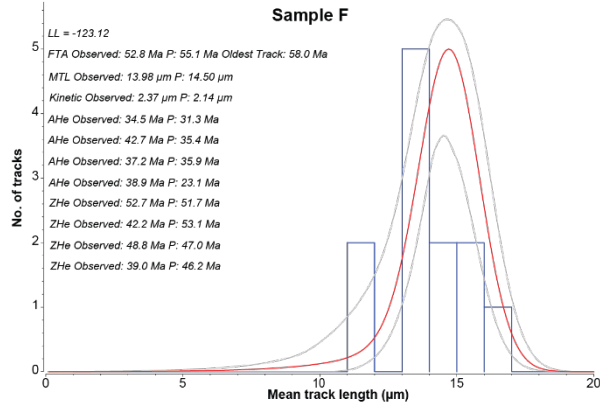




**Figure S9.** Predicted versus observed for thermal history modeling of Samples C and F (this study) and those of Flowers et al., 2008. AHe – apatite (U-Th-Sm)/He; FTA – fission-track analysis; MTL – mean track length; LL – log-likelihood; Kinetic is Dpar.

## REFERENCES CITED

- Black, L.P., Kamo, S.L., Allen, C.M., Davis, D.W., Aleinikoff, J.N., Valley, J.W., Mundil, R., Campbell, I.H., Korsch, R.J., and Williams, I.S., 2004, Improved  $^{206}\text{Pb}/^{238}\text{U}$  microprobe geochronology by the monitoring of a trace-element-related matrix effect; SHRIMP, ID-TIMS, ELA-ICP-MS and oxygen isotope documentation for a series of zircon standards: *Chemical Geology*, v. 205, p. 115-140.
- Braun, J., van der Beek, P., and Batt, G., 2006, *Quantitative thermochronology: Numerical methods for the interpretation of thermochronological data*: Cambridge University Press, 272 p.
- Donelick, R.A., O'Sullivan, P.B., and Ketcham, R.A., 2005, Apatite fission-track analysis: *Reviews in Mineralogy and Geochemistry*, v. 58, p. 49-94,  
<https://doi.org/10.2138/rmg.2005.58.3>.
- Dumańska-Słowik, M., Weselucha-Birczyńska, A., and Pieczka, A., 2015, Micas from mariupolite of the Oktiabrski massif (SE Ukraine): An insight into the host rock evolution – Geochemical data supported by Raman microspectroscopy: *Spectrochimica Acta Part A: Molecular and Biomolecular Spectroscopy*, v. 137, p. 817-826,  
<https://doi.org/10.1016/j.saa.2014.08.127>.
- Farley, K.A., 2002, (U-Th)/He dating: techniques, calibrations, and applications: *Reviews of Mineralogy and Geochemistry*, v. 47, p. 819–844,  
<https://doi.org/10.2138/rmg.2002.47.18>.

- Flowers, R.M., Farley, K.A., and Ketcham, R.A., 2015, A reporting protocol for thermochronologic modeling illustrated with data from the Grand Canyon: Earth and Planetary Science Letters, v. 432, p. 425-435, <https://doi.org/10.1016/j.epsl.2015.09.053>.
- Flowers, R.M., Ketcham, R.A., Enkelmann, E., Gautheron, C., Reiners, P.W., Metcalf, J.R., Danišik, M., Stockli, D.F., and Brown, R. W., 2023, (U-Th)/He chronology: Part 2. Considerations for evaluating, integrating, and interpreting conventional individual aliquot data: GSA Bulletin, v. 135, p. 137-161, <https://doi.org/10.1130/B36268.1>.
- Flowers, R. M., Wernicke, B. P., and Farley, K. A., 2008, Unroofing, incision, and uplift history of the southwestern Colorado Plateau from apatite (U-Th)/He thermochronometry: Geological Society of America Bulletin, v. 120, p. 571-587, <https://doi.org/10.1130/B26231.26231>.
- Gallagher, K., 2012, Transdimensional inverse thermal history modeling for quantitative thermochronology: Journal of Geophysical Research, v. 117, <https://doi.org/10.1029/2011JB008825>.
- Gautheron, C., Tassan-Got, L., Ketcham, R.A., and Dobson, K.J., 2012, Accounting for long alpha-particle stopping distances in (U-Th-Sm)/He geochronology: 3D modeling of diffusion, zoning, implantation, and abrasion: Geochimica et Cosmochimica Acta, v. 96, p. 44–56, <https://doi.org/10.1016/j.gca.2012.08.016>.
- Gehrels, G., and Pecha, M., 2014, Detrital zircon U-Pb geochronology and Hf isotope geochemistry of Paleozoic and Triassic passive margin strata of western North America: Geosphere, v. 10, p. 49-65.
- Gehrels, G.E., Valencia, V.A., and Ruiz, J., 2008, Enhanced precision, accuracy, efficiency, and spatial resolution of U-Pb ages by laser ablation–multicollector–inductively coupled

- plasma–mass spectrometry: *Geochemistry, Geophysics, Geosystems*, v. 9, Q03017, <https://doi.org/10.1029/2007GC001805>.
- Gleadow, A.J.W., Hurford, A.J., and Quaife, R.D., 1976, Fission track dating of zircon: Improved etching techniques. *Earth and Planetary Science Letters* v. 33, p. 273–276.
- He, J.J.Y., and Reiners, P.W., 2022, A revised alpha-ejection correction calculation for (U–Th)/He thermochronology dates of broken apatite crystals: *Geochronology*, v. 4, p. 629–640, <https://doi.org/10.5194/gchron-4-629-2022>.
- He, J.J.Y., Thomson, S.N., Reiners, P.W., Hemming, S.R., and Licht, K.J., 2021, Rapid erosion of the central Transantarctic Mountains at the Eocene-Oligocene transition: Evidence from skewed (U–Th)/He date distributions near Beardmore Glacier: *Earth and Planetary Science Letters*, v. 567, 117009, <https://doi.org/10.1016/j.epsl.2021.117009>.
- Hurford, A.J., and Green, P.F., 1983, The zeta age calibration of fission-track dating: *Chemical Geology*, v. 41, p. 285–317.
- Ketcham, R.A., Carter, A., Donelick, R.A., Barbarand, J., and Hurford, A.J., 2007, Improved modeling of fission-track annealing in apatite: *American Mineralogist*, v. 92, p. 799-810, <https://doi.org/10.2138/am.2007.2281>
- Kuiper, K.F., Deino, A., Hilgen, F.J., Krijgsman, W., Renne, P.R., and Wijbrans, J.R., 2008, Synchronizing rocks clocks of Earth history: *Science*, v. 320, p. 500-504.
- Lee, J.-Y., Marti, K., Severinghaus, J.P., Kawamura, K., Yoo, H.-S., Lee, J.B., and Kim, J.S., 2006, A redetermination of the isotopic abundances of atmospheric Ar. *Geochimica et Cosmochimica Acta*, v. 70, p. 4507-4512.
- Min, K., Mundil, R., Renne, P.R., and Ludwig, K.R., 2000, A test for systematic errors in  $^{40}\text{Ar}/^{39}\text{Ar}$  geochronology through comparison with U/Pb analysis of a 1.1-Ga rhyolite: *Geochimica et Cosmochimica Acta*, v. 64, p. 73-98.

- Paces, J.B., and Miller Jr, J.D., 1993, Precise U-Pb ages of Duluth complex and related mafic intrusions, northeastern Minnesota: Geochronological insights to physical, petrogenetic, paleomagnetic, and tectonomagmatic processes associated with the 1.1 Ga midcontinent rift system: *Journal of Geophysical Research: Solid Earth*, v. 98, p. 13997-14013.
- Pullen, A., Ibáñez-Mejía, M., Gehrels, G.E., Giesler, D., and Pecha, M., 2018, Optimization of a laser ablation-single collector-inductively coupled plasma-mass Spectrometer (Thermo Element 2) for accurate, precise, and efficient zircon U-Th-Pb geochronology: *Geochemistry, Geophysics, Geosystems*, v. 19, p. 3689-3705.
- Reiners, P.W., Carlson, R.W., Renne, P.R., Cooper, K.M., Granger, D.E., McLean, N.M., and Schoene, B., 2018, *Geochronology and Thermochronology*: Oxford, John Wiley and Sons Ltd., 464 p.
- Ritz, M., and Valášková, M., 2018, Infrared and Raman spectroscopy of three commercial vermiculites doped with cerium dioxide nanoparticles: *Spectrochimica Acta Part A: Molecular and Biomolecular Spectroscopy*, v. 201, p. 39-45, <https://doi.org/10.1016/j.saa.2018.04.053>.
- Ross, J., 2019, NMGR/PyChron v18.2: Zenodo, <https://doi.org/10.5281/zenodo.3237834>.
- Spiegel, C., Kohn, B., Belton, D., Berner, Z., and Gleadow, A., 2009, Apatite (U-Th-Sm)/He thermochronology of rapidly cooled samples: the effect of He implantation: *Earth and Planetary Science Letters*, v. 285, p. 105–114, <https://doi.org/10.1016/j.epsl.2009.05.045>.
- Stacey, J.T., and Kramers, J., 1975, Approximation of terrestrial lead isotope evolution by a two-stage model: *Earth and planetary science letters*, v. 26, p. 207-221.
- Vermeesch, P., 2009, RadialPlotter: a Java application for fission track, luminescence and other radial plots: *Radiation Measurements*, v. 44, p. 409-410.
- Wang, A., Freeman, J.J., and Jolliff, B.L., 2015, Understanding the Raman spectral features of phyllosilicates: *Journal of Raman Spectroscopy*, <https://doi.org/10.1002/jrs.4680>.